Developmental Cell
Article

Dual Role of Mitofilin in Mitochondrial Membrane Organization and Protein Biogenesis

Karina von der Malsburg,[1,2,13] Judith M. Müller,[1,3,13] Maria Bohnert,[1,3,13] Silke Oeljeklaus,[2,4] Paulina Kwiatkowska,[6,7] Thomas Becker,[1,2] Adrianna Loniewska-Lwowska,[6,14] Sebastian Wiese,[2,4] Sanjana Rao,[1,3,5] Dusanka Milenkovic,[1,15] Dana P. Hutu,[1,16] Ralf M. Zerbes,[1] Agnes Schulze-Specking,[1,2] Helmut E. Meyer,[8] Jean-Claude Martinou,[9] Sabine Rospert,[1,2] Peter Rehling,[10,11] Chris Meisinger,[1,2] Marten Veenhuis,[12] Bettina Warscheid,[2,4] Ida J. van der Klei,[12] Nikolaus Pfanner,[1,2,*] Agnieszka Chacinska,[1,6,*] and Martin van der Laan[1,2]
[1]Institut für Biochemie und Molekularbiologie, ZBMZ
[2]BIOSS Centre for Biological Signalling Studies
[3]Fakultät für Biologie
[4]Institut für Biologie II, Funktionelle Proteomik
[5]SGBM Spemann Graduate School of Biology and Medicine
Universität Freiburg, 79104 Freiburg, Germany
[6]International Institute of Molecular and Cell Biology, 02-109 Warsaw, Poland
[7]Warsaw University of Technology, 00-661 Warsaw, Poland
[8]Medizinisches Proteom-Center, Ruhr-Universität Bochum, 44801 Bochum, Germany
[9]Departement de Biologie Cellulaire, University of Geneva, 1211 Geneva, Switzerland
[10]Abteilung Biochemie II, Universität Göttingen, 37073 Göttingen, Germany
[11]Max Planck Institute for Biophysical Chemistry, 37077 Göttingen, Germany
[12]Groningen Biomolecular Sciences & Biotechnology Institute, University of Groningen, Kluyver Centre for Genomics of Industrial Fermentation, 9700 CC Groningen, The Netherlands
[13]These authors contributed equally to this work
[14]Present address: Medical Centre for Postgraduate Education, 01-813 Warsaw, Poland
[15]Present address: Max Planck Institute for Biology of Ageing, 50931 Cologne, Germany
[16]Present address: European Commission, Joint Research Centre, Institute for Reference Materials and Measurements, 2440 Geel, Belgium
*Correspondence: Nikolaus.Pfanner@biochemie.uni-freiburg.de (N.P.), achacinska@iimcb.gov.pl (A.C.)
DOI 10.1016/j.devcel.2011.08.026

SUMMARY

The mitochondrial inner membrane consists of two domains, inner boundary membrane and cristae membrane that are connected by crista junctions. Mitofilin/Fcj1 was reported to be involved in formation of crista junctions, however, different views exist on its function and possible partner proteins. We report that mitofilin plays a dual role. Mitofilin is part of a large inner membrane complex, and we identify five partner proteins as constituents of the *m*itochondrial *in*ner membrane *o*rganizing *s*ystem (MINOS) that is required for keeping cristae membranes connected to the inner boundary membrane. Additionally, mitofilin is coupled to the outer membrane and promotes protein import via the mitochondrial intermembrane space assembly pathway. Our findings indicate that mitofilin is a central component of MINOS and functions as a multifunctional regulator of mitochondrial architecture and protein biogenesis.

INTRODUCTION

Mitochondria are double-membrane bound, ubiquitous organelles that contain more than 1,000 different proteins and fulfill numerous functions in the physiology of eukaryotic cells (Dolezal et al., 2006; Neupert and Herrmann, 2007; Chacinska et al., 2009; Endo et al., 2011). Most mitochondrial proteins are encoded in the nucleus and synthesized on cytosolic ribosomes as precursor proteins with distinct import signals. The translocase of the outer membrane (TOM complex) constitutes the main entry gate for virtually all mitochondrial precursor proteins. From the TOM complex precursors are routed to downstream protein sorting machineries of the different mitochondrial subcompartments (summarized in Dolezal et al., 2006; Neupert and Herrmann, 2007; Chacinska et al., 2009; Endo et al., 2011). The sorting and assembly machinery (SAM complex) mediates the integration of β-barrel precursor proteins into the outer mitochondrial membrane. The mitochondrial intermembrane space assembly machinery (MIA) guides cysteine-rich proteins into the intermembrane space. Precursor proteins with N-terminal cleavable presequences are translocated by the presequence translocase of the inner membrane (TIM23 complex). Metabolite carriers are bound to TIM chaperones in the intermembrane space and are inserted into the inner membrane by the carrier translocase (TIM22 complex).

The inner mitochondrial membrane consists of two morphologically distinct regions: the inner boundary membrane, which is in close proximity to the outer membrane, and large tubular invaginations, termed cristae membranes (Mannella, 2006; Zick et al., 2009). Several studies have indicated that inner boundary membrane and cristae membrane domains are distinct subcompartments of the inner membrane, as they exhibit an asymmetric protein distribution (Vogel et al., 2006; Wurm and Jakobs, 2006; Zick et al., 2009). Direct but transient interactions

between outer membrane TOM complexes and inner boundary membrane-located TIM23 complexes facilitate transfer of presequence-carrying preproteins from the outer to the inner membrane (Chacinska et al., 2005; Tamura et al., 2009; Mokranjac et al., 2009). The extended cristae membrane structures are the main sites of ATP synthesis by oxidative phosphorylation (Gilkerson et al., 2003; Vogel et al., 2006; Wurm and Jakobs, 2006). It has been suggested that the typical architecture of cristae provides a specific microenvironment that enhances the catalytic capacity of the OXPHOS system (Mannella, 2006; Strauss et al., 2008). The border regions between inner boundary membrane and cristae membranes have been termed crista junctions. Based on morphological characterization by electron microscopy, crista junction structures are narrow tubular openings with a defined diameter and length and high membrane curvature (Renken et al., 2002; Mannella, 2006; Rabl et al., 2009; Zick et al., 2009).

Aberrant cristae morphologies have been observed in yeast mutants that are unable to assemble F_1F_o-ATP synthase dimers and oligomers (Paumard et al., 2002). The dynamin-like GTPase Mgm1/OPA1, which functions in mitochondrial fusion, has also been shown to be involved in cristae morphogenesis (Arnoult et al., 2005; Frezza et al., 2006; Meeusen et al., 2006; Yamaguchi et al., 2008). Prohibitins likely function in this process through regulation of Mgm1/OPA1 processing (Merkwirth et al., 2008). John et al. (2005) identified mitofilin as a key player in the control of cristae morphology. Knockdown of mitofilin induced a massive increase of the inner membrane surface accompanied by the formation of large concentric stacks of cristae membranes and loss of crista junctions. A similar phenotype was observed in yeast cells lacking the mitofilin ortholog Fcj1, suggesting that mitofilin/Fcj1 promotes the formation of crista junctions (Rabl et al., 2009). Mitofilin is found in high molecular weight complexes (John et al., 2005; Xie et al., 2007; Rabl et al., 2009). Different views of potential interaction partners of mitofilin were reported (Xie et al., 2007; Mun et al., 2010; Darshi et al., 2011), although the main studies addressing mitofilin functions reported that mitofilin is engaged in homotypic interactions (John et al., 2005; Rabl et al., 2009). Currently, the molecular context, in which mitofilin acts in cristae morphogenesis, is unknown.

For this study, we performed a systematic analysis of mitofilin partner proteins. We report that mitofilin is part of a large multisubunit protein complex in the inner membrane, termed *m*itochondrial *in*ner membrane *o*rganizing *s*ystem (MINOS) for its role in controlling cristae morphology. Additionally, mitofilin interacts with the TOM complex and promotes protein import into the intermembrane space via the MIA pathway.

RESULTS

Mitofilin Interacts with the TOM Complex

Mitofilin is anchored in the inner mitochondrial membrane by an N-terminal transmembrane segment (John et al., 2005; Rabl et al., 2009). Its large hydrophilic part, which contains predicted coiled-coil regions and a conserved C-terminal mitofilin domain, is exposed to the intermembrane space (see Figure S1, available online). For an initial screening for possible partner proteins of mitofilin, we fused a Protein A-tag to the C terminus of yeast mitofilin (Fcj1) and performed affinity purification mass spectrometry based on stable isotope labeling with amino acids in cell culture (SILAC) (Ong and Mann, 2006). Yeast cells expressing $Fcj1_{ProtA}$ were grown in minimal medium in the presence of standard amino acids, whereas a wild-type yeast strain was labeled by the addition of [$^{13}C/^{15}N$]lysine and [$^{13}C/^{15}N$]arginine to the growth medium. Mitochondria were isolated from both strains, solubilized by digitonin and subjected to IgG affinity chromatography. Elution fractions were pooled and analyzed by mass spectrometry. Putative interaction partners of Fcj1 were selected according to the enrichment of "light" peptides ($^{12}C/^{14}N$) originating from the $Fcj1_{ProtA}$ samples over "heavy" peptides ($^{13}C/^{15}N$) derived from the wild-type control samples. This analysis identified a number of possible candidate proteins, which included proteins involved in respiration, metabolite carriers and so far uncharacterized proteins (Table S1). Surprisingly, among the most enriched proteins were two core components of the TOM complex, the channel-forming protein Tom40 and the central receptor Tom22. This finding raised the possibility of a link between mitofilin and the outer membrane.

We analyzed the eluates of $Fcj1_{ProtA}$ affinity purification by specific antibodies. Both Tom40 and Tom22 were copurified with Fcj1 (Figures 1A and 1B). Subunits of the preprotein translocases of the inner membrane, the respiratory complexes II, III, and IV and the F_1F_o-ATP synthase were not detected in substantial amounts in the eluates (Figure 1A). Separation of the eluates by blue native electrophoresis revealed that the intact TOM complex, and not only individual subunits, was copurified with Fcj1 (Figure 1C).

To exclude that the interaction of TOM with Fcj1 occurs only after solubilization of mitochondria we performed postlysis control experiments (Figure 1B). Radiolabeled Tom40 was imported into mitochondria isolated from $Fcj1_{ProtA}$ or wild-type cells. $Fcj1_{ProtA}$ mitochondria loaded with [^{35}S]Tom40 were mixed with unlabeled wild-type mitochondria. After lysis and affinity chromatography, [^{35}S]Tom40 was observed in the eluate like endogenous (unlabeled) Tom40 (Figure 1B, lane 6). However, when wild-type mitochondria loaded with [^{35}S]Tom40 were mixed with unlabeled $Fcj1_{ProtA}$ mitochondria, [^{35}S]Tom40 was not detected in the eluate (Figure 1B, lane 5), demonstrating that [^{35}S]Tom40 did not bind to $Fcj1_{ProtA}$ after lysis of the mitochondria. These data demonstrate that mitofilin interacts with the TOM complex in organello.

Lack of Mitofilin Impairs Protein Import via the MIA Pathway

We asked if the interaction of mitofilin/Fcj1 with the TOM complex may reveal a connection of Fcj1 to mitochondrial preprotein import. Mitochondria, which were isolated from a yeast strain lacking Fcj1, were incubated with different radiolabeled precursor proteins that are transported into or across the inner membrane: the inner-membrane-targeted model preprotein b_2-DHFR and the matrix-targeted β subunit of F_1-ATPase ($F_1β$) are imported via the TIM23 complex and proteolytically processed (Figure 2A) (Chacinska et al., 2005); the precursor of the ADP/ATP carrier (AAC) is imported via the TIM22 complex and assembles to the mature dimer (Figure 2B) (Chacinska et al., 2009). These preproteins were imported into *fcj1Δ* mitochondria in a membrane potential ($Δψ$)-dependent manner; the

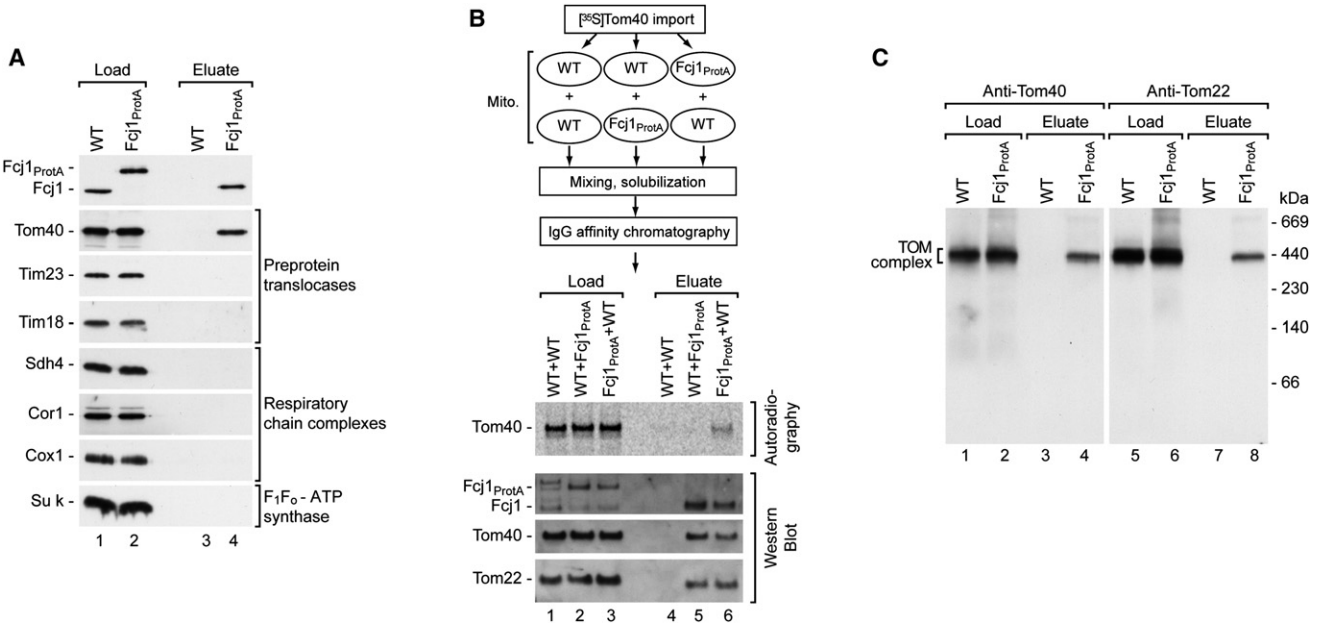

Figure 1. Mitofilin/Fcj1 Interacts with the TOM Complex

(A) Digitonin-solubilized wild-type (WT) and Fcj1$_{ProtA}$ yeast mitochondria were subjected to IgG affinity chromatography, elution with TEV protease, and analysis by SDS-PAGE and immunoblotting. Load, 4%; eluate, 100%.

(B) ^{35}S-labeled Tom40 was imported into wild-type or Fcj1$_{ProtA}$ mitochondria as indicated and precursor-loaded mitochondria were mixed with unlabeled wild-type or Fcj1$_{ProtA}$ mitochondria prior to solubilization with digitonin. Extracts were subjected to IgG affinity chromatography. Samples were analyzed by autoradiography and western blotting. Load, 0.5%; eluate, 100%.

(C) WT and Fcj1$_{ProtA}$ mitochondria were subjected to affinity chromatography as in (A). Samples were analyzed by blue native electrophoresis. Load, 3%; eluate, 100%. See also Figure S1 and Table S1.

import efficiency was moderately reduced compared to wild-type mitochondria (Figures 2A and 2B). The $\Delta\psi$ of *fcj1Δ* mitochondria was also moderately reduced (Rabl et al., 2009) (Figure 2C), leading to a reduced import efficiency of preproteins that are transported into or across the inner membrane. Thus, we did not obtain evidence that Fcj1 itself is connected to protein import into the inner membrane or matrix, but the lack of Fcj1 indirectly affects import of presequence-carrying and carrier precursors via a partial reduction of $\Delta\psi$.

Finally, we analyzed the third protein import pathway that employs an inner membrane component, the MIA pathway (Neupert and Herrmann, 2007; Chacinska et al., 2009; Endo et al., 2011). Yeast Mia40 (Tim40) is an inner membrane protein with a large intermembrane space receptor domain. MIA substrates are small intermembrane space proteins containing characteristic cysteine motifs, such as the precursors of small Tim proteins. The precursors are translocated across the outer membrane into the intermembrane space and thus their import does not require a $\Delta\psi$ across the inner membrane. Mia40 transiently binds its substrates in the form of disulfide-linked import intermediates (Milenkovic et al., 2007; Sideris and Tokatlidis, 2007; Stojanovski et al., 2008; Kawano et al., 2009). Mia40 cooperates with the sulfhydryl oxidase Erv1 to complete import and oxidative folding of substrate proteins (Stojanovski et al., 2008; Tienson et al., 2009; Bien et al., 2010). Strikingly, the import of MIA substrates to a protease-protected location was strongly impaired in *fcj1Δ* mitochondria, as analyzed with in vitro synthesized ^{35}S-labeled Tim9 and recombinant Tim10 precursor (Figure 2D). The steady-state levels of Mia40 were similar in *fcj1Δ* and wild-type mitochondria (Figure S2A). Moreover, the lack of Fcj1 did not alter the redox state of Mia40 as the ratio between oxidized and partially reduced Mia40 was not affected (Figure S2B, lanes 3 and 4) (Mia40 was fully reduced by dithiothreitol (DTT) under denaturing conditions; Figure S2B, lanes 1 and 2).

To determine at which stage the MIA pathway was impaired in *fcj1Δ* mitochondria, we dissected the import stages by use of blue native electrophoresis. The precursor of Tim9 first forms an import intermediate with Mia40 and then assembles into the mature Tim9-Tim10 and TIM22 complexes (Stojanovski et al., 2008) (Figure 2E, lanes 1–3). The lack of Fcj1 already impaired the formation of the Tim9-Mia40 intermediate; the subsequent assembly steps were similarly inhibited (Figure 2E, lanes 4–6). Dissipation of $\Delta\psi$ neither affected the import of Tim9 in wild-type nor in *fcj1Δ* mitochondria (Figure 2E, lanes 7–12), excluding that the partial reduction of $\Delta\psi$ in *fcj1Δ* mitochondria was responsible for the observed import inhibition. The import pathway of Tim8 can be dissected into a Mia40-intermediate, formation of oxidized Tim8 and assembly into the Tim8-Tim13 complex. These steps, including the initial Tim8-Mia40 intermediate, were impaired in *fcj1Δ* mitochondria (Figure 2E, lanes 16–18). We conclude that mitochondria lacking mitofilin/Fcj1 are impaired in import of precursor proteins into the intermembrane space via the MIA pathway.

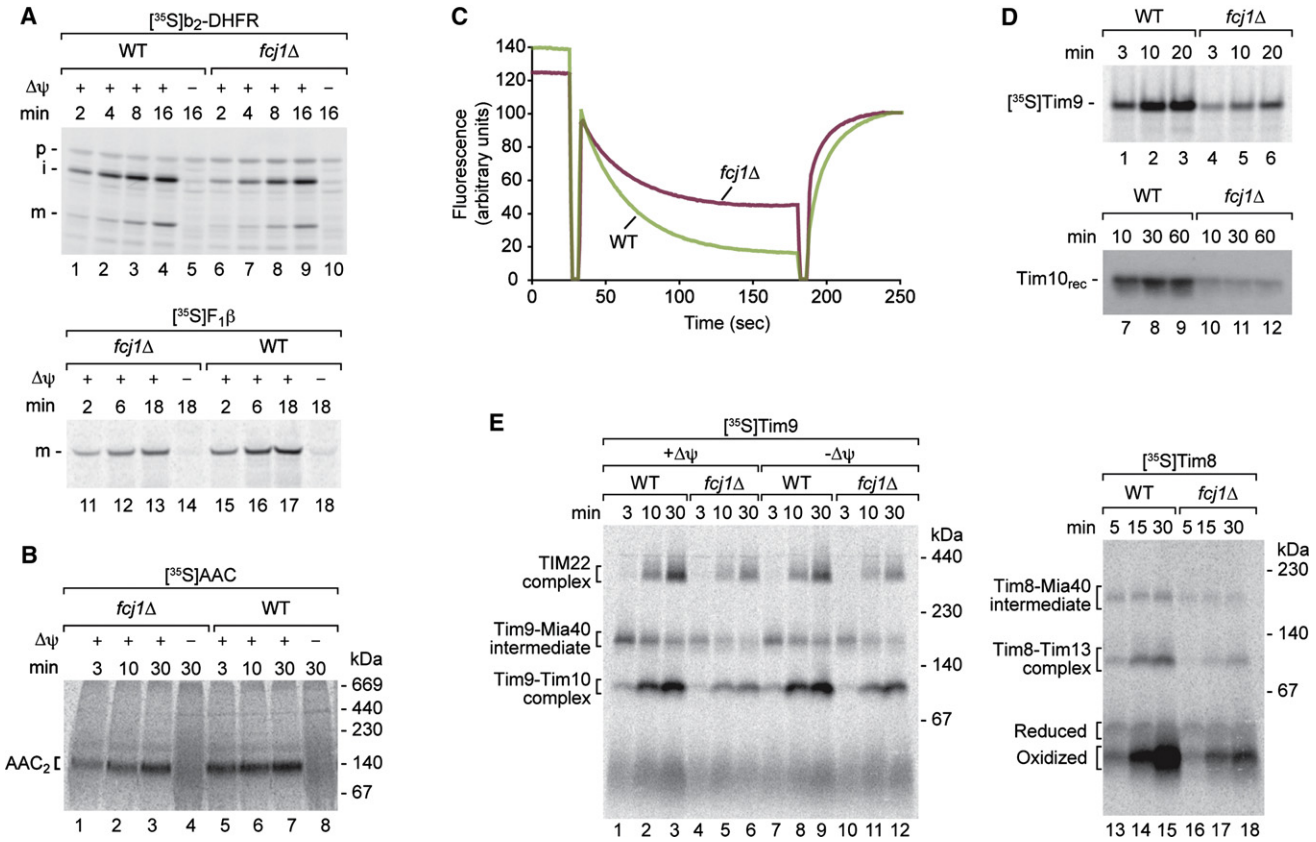

Figure 2. Lack of Mitofilin/Fcj1 Impairs Protein Import into the Intermembrane Space

(A) Import of ^{35}S-labeled b_2-DHFR and $F_1\beta$ into wild-type (WT) and *fcj1Δ* mitochondria, followed by treatment with proteinase K. p, precursor; i, intermediate; m, mature.

(B) ^{35}S-labeled AAC was imported into wild-type and *fcj1Δ* mitochondria and formation of the mature form (AAC_2) was monitored by blue native electrophoresis.

(C) Inner membrane potential of wild-type and *fcj1Δ* mitochondria was measured using a potential-sensitive fluorescent dye.

(D) Import of ^{35}S-labeled Tim9 or recombinant, purified $Tim10_{His}$ into wild-type and *fcj1Δ* mitochondria, followed by treatment with proteinase K.

(E) After incubation with ^{35}S-labeled Tim9 or Tim8, wild-type, and *fcj1Δ* mitochondria were solubilized with digitonin and analyzed by blue native electrophoresis.

See also Figure S2.

MINOS—Inner Membrane Partner Proteins of Mitofilin

We asked how mitofilin might affect the MIA pathway. Loss of mitofilin/Fcj1 leads to characteristic alterations of the morphology of the inner mitochondrial membrane with large stacks of cristae membrane sheets and loss of crista junctions (John et al., 2005; Rabl et al., 2009; Mun et al., 2010). Thus, a portion of the intermembrane space (intracristal space) apparently becomes segregated in these cristae stacks and we reasoned that the morphological perturbations in *fcj1*Δ mitochondria may interfere with protein import into the intermembrane space. To address this possibility we went back to our initial screen for potential interaction partners of Fcj1 (Table S1). Several candidate proteins with hitherto unknown function were found in this screen. We reasoned that some of these proteins might cooperate with Fcj1 in the control of cristae morphology and thus may also affect the MIA pathway. We raised antibodies against these proteins to test for a possible association with Fcj1 by affinity chromatography experiments. Strikingly, five so far uncharacterized yeast proteins identified in our initial screen were efficiently copurified with $Fcj1_{ProtA}$ (Figure 3A). A large number of further proteins, including metabolite carriers and proteins of respiratory complexes, were either not copurified with Fcj1 or found in only small amounts in the eluate (Figure 3A) (a small but reproducible fraction of the external NADH dehydrogenase, analyzed with antibodies against Nde1, was observed in the eluate).

Three of the identified Fcj1-interactors, Aim5, Aim13, and Aim37, were found in a screen for proteins that affect mitochondrial inheritance (*a*ltered *i*nheritance of *m*itochondria) but were not further analyzed (Hess et al., 2009). The two other interactors are encoded by the open reading frames *YCL057C-A* and *YGR235C*; we named the proteins Mio10 and Mio27 for *m*itochondrial *i*nner membrane *o*rganization components of 10 kDa and 27 kDa, respectively.

We localized Fcj1 and the five interactors Aim5, Aim13, Aim37, Mio10, and Mio27 by subfractionation of mitochondria. The proteins were not accessible to proteinase K added to isolated mitochondria (Figure 3B, lane 2). When the outer membrane was opened by osmotic swelling (generation of mitoplasts), the proteins became accessible to the protease, indicating that they expose domains to the intermembrane space comparable to control proteins like Tim21 (Figure 3B, lane 4). Washing of

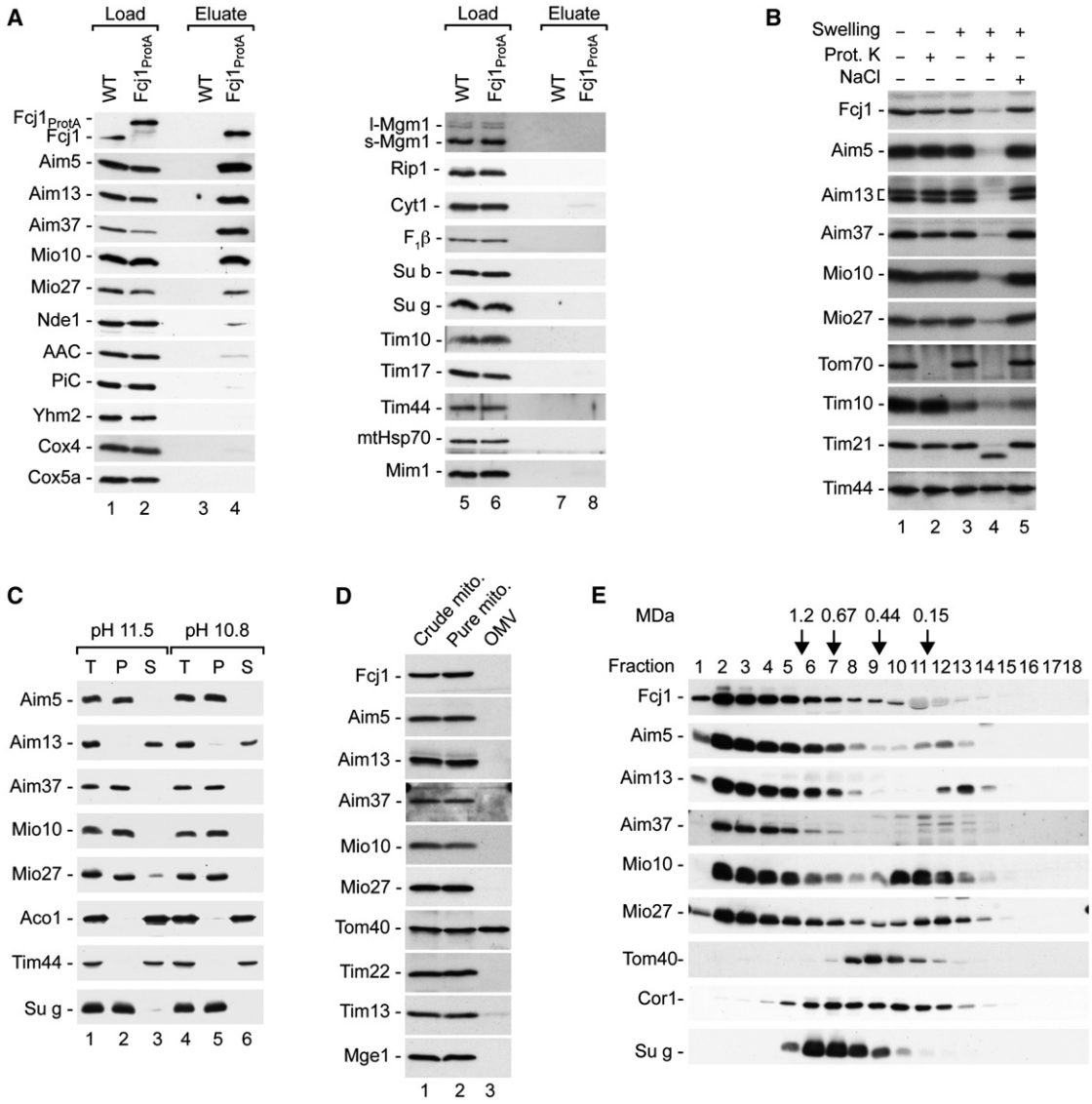

Figure 3. Inner Membrane Partner Proteins of Mitofilin/Fcj1

(A) IgG affinity chromatography with digitonin-solubilized wild-type (WT) and $Fcj1_{ProtA}$ mitochondria and western blot analysis. PiC, phosphate carrier; l-Mgm1, long form of Mgm1; s-Mgm1, short form of Mgm1; Su b/Su g, subunits b and g of F_1F_o-ATP synthase. Load, 4%; eluate, 100%.

(B) Isolated mitochondria were diluted in hypoosmotic buffer (Swelling) and treated with Proteinase K (Prot. K) or 500 mM NaCl as indicated.

(C) Separation of soluble and membrane-integral proteins by incubation of mitochondria in Na_2CO_3 solutions of pH 11.5 or 10.8 followed by ultracentrifugation. Total (T), pellet (P), and supernatant (S) fractions were analyzed by SDS-PAGE and immunoblotting.

(D) Protein content of crude and highly purified wild-type mitochondria and isolated outer mitochondrial membrane vesicles (OMV).

(E) Digitonin-solubilized wild-type mitochondria were analyzed by size exclusion chromatography, SDS-PAGE, and immunodecoration. See also Figure S1 and Table S1.

mitoplasts with a high salt buffer did not lead to extraction of the proteins, indicating that they are membrane-associated (Figure 3B, lane 5). When mitochondria were subjected to alkaline extraction, Fcj1, Aim5, Aim37, Mio10, and Mio27 were recovered in the pellet fraction together with the control protein subunit g of the F_1F_o-ATP synthase, indicating that they are integral inner membrane proteins (Figure 3C). In contrast, Aim13 was found in the supernatant fraction together with control proteins like Tim44 (Figure 3C). Because Aim13 was not released from mitochondria upon osmotic swelling, but became accessible to added protease (Figure 3B), we conclude that Aim13 is a peripheral membrane protein exposed to the intermembrane space. To directly determine if Fcj1 and the interactors Aim5, Aim13, Aim37, Mio10, and Mio27 are located in the outer or inner membrane, we purified mitochondrial outer membrane vesicles and compared them to crude and gradient-purified mitochondria (Figure 3D). None of the proteins was found in the outer membrane fraction (with the marker protein Tom40), indicating that they are inner membrane proteins like the control protein Tim22 (the Fcj1-TOM interaction across two membranes is

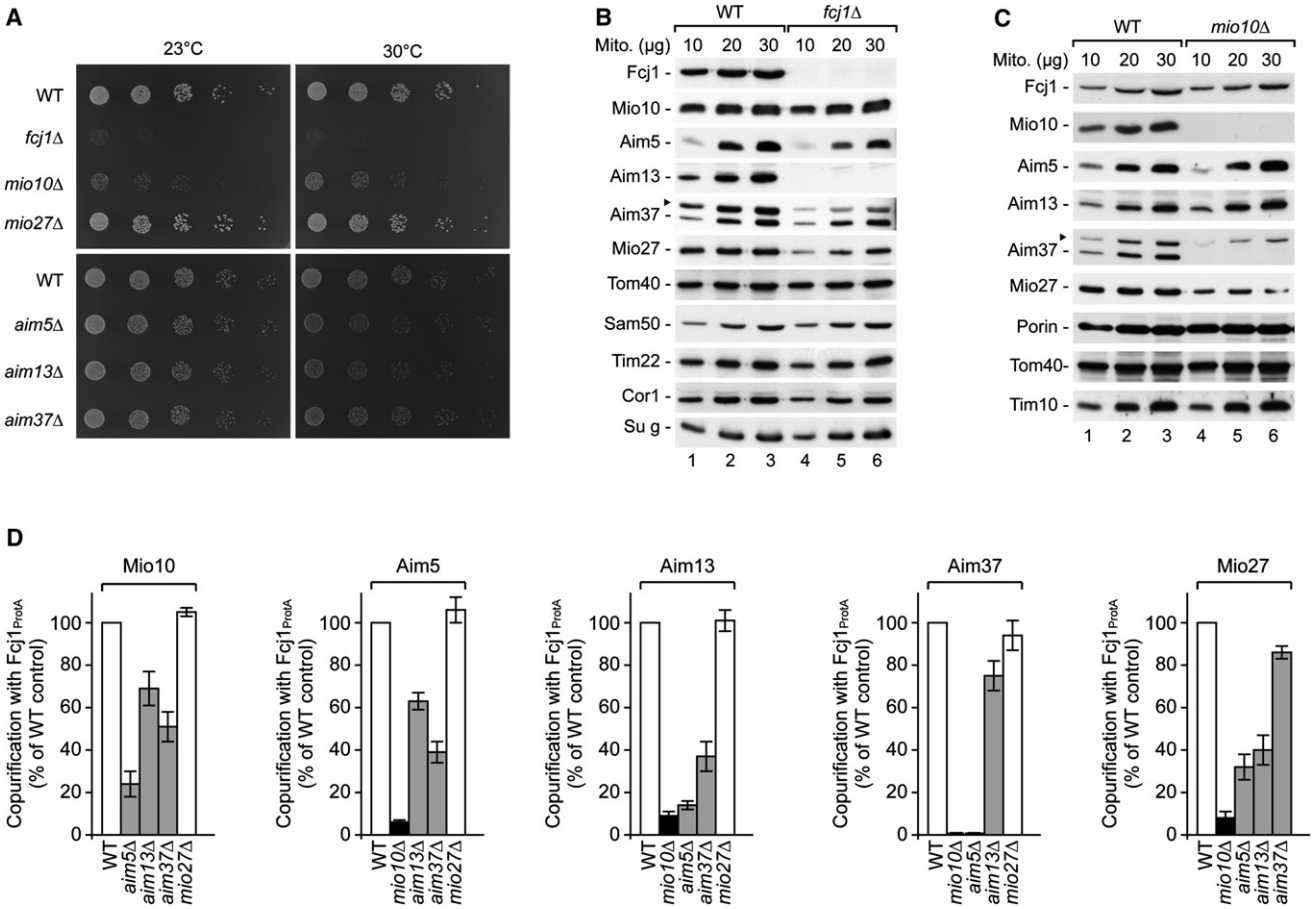

Figure 4. Mitofilin/Fcj1 and Mio10 as Core Components of MINOS

(A) Serial dilutions of wild-type (WT) and mutant yeast strains on synthetic complete medium containing 3% glycerol incubated at 23°C or 30°C.

(B and C) Protein levels of wild-type, *fcj1*Δ and *mio10*Δ mitochondria analyzed by SDS-PAGE and immunoblotting. Arrowhead, unspecific band.

(D) Comprehensive quantitative analysis of the interdependence of MINOS proteins with respect to their association with Fcj1 normalized to the expression levels of the proteins and the efficiency of bait recovery. Data are represented as mean ± SEM (n = 3). See also Figure S3.

disrupted during the procedure of outer membrane purification). As expected soluble control proteins like Tim13 (intermembrane space) or Mge1 (matrix) were also not detected in considerable amounts in the outer membrane fraction. Taken together, Aim5, Aim37, Mio10, and Mio27 behave as integral inner membrane proteins that expose domains to the intermembrane space, like Fcj1. In agreement with this localization, one (Aim5) or two (Mio10, Aim37, Mio27) hydrophobic transmembrane segments are predicted for these proteins (Figure S1). Aim37 and Mio27 are homologous to each other (17.4% identity/41.3% similarity). Aim13, for which no transmembrane segment is predicted, behaves as peripheral inner membrane protein located on the intermembrane space side.

It has been suggested that mitofilin/Fcj1 forms a large protein complex in the inner membrane by homotypic interactions (John et al., 2005; Rabl et al., 2009). We performed size exclusion chromatography using digitonin-solubilized mitochondria and observed that the major pools of the five inner membrane-located interactors comigrated with Fcj1 in the high molecular weight range (Figure 3E, fractions 2–5). A comparison with the migration behavior of F_1F_o-ATP synthase complexes and respiratory chain supercomplexes (formed by bc_1-complex and cytochrome *c* oxidase) revealed a large size for Fcj1 and its interactors with a migration in the MDa range. We named the system of Fcj1 and its inner membrane partner proteins MINOS for mitochondrial inner membrane organizing system.

Mitofilin and Mio10 Are Core Components of MINOS

We analyzed yeast strains where the genes for individual MINOS proteins were deleted. *fcj1*Δ and *mio10*Δ cells showed strong growth defects on nonfermentable medium; *aim5*Δ and *aim13*Δ cells showed a minor growth delay at 30°C; *aim37*Δ and *mio27*Δ cells, as well as a *aim37*Δ *mio27*Δ double mutant grew similarly like wild-type cells under the conditions analyzed (Figure 4A; Figure S3A). Mitochondria were isolated from the single deletion strains and the steady-state levels of MINOS components and control proteins were analyzed. Lack of Fcj1 led to a loss of Aim13 and a moderate reduction of the levels of Aim5, Aim37, and Mio27, whereas the levels of Mio10 and control proteins were unchanged (Figure 4B). In mitochondria prepared from the *mio10*Δ strain, Aim37 was not detectable and the levels of Mio27 were moderately reduced, whereas other

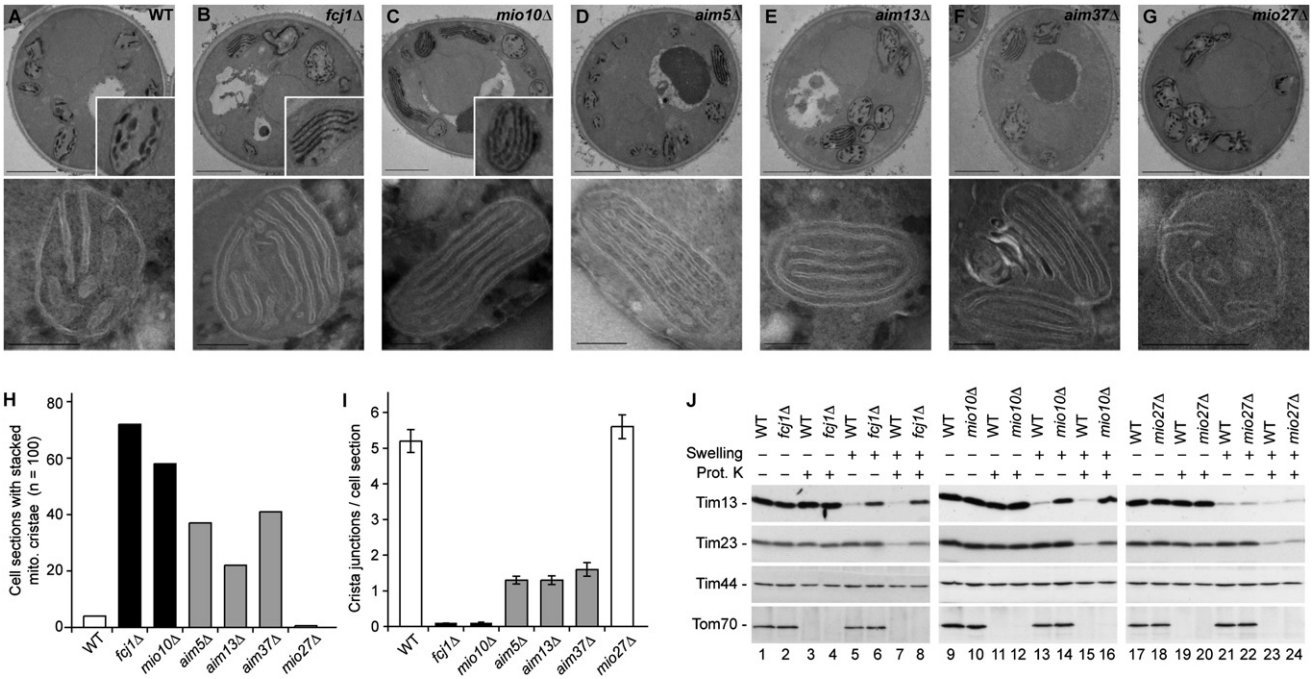

Figure 5. Morphological Alteration of Mitochondrial Inner Membrane in MINOS Mutants

(A–G) Representative electron microscopy images of mitochondrial ultrastructures in WT and yeast deletion mutant strains. Upper row: diaminobenzidine (DAB) staining (bar represents 1 μm), lower row: negative stain cryoelectron microscopy (bar represents 200 nm).

(H) Quantification of WT and mutant cell sections with stacked mitochondrial cristae membranes based on DAB-stained sections (n = 100).

(I) Quantitative analysis of crista junctions observed per DAB-stained cell section. Data are represented as mean ± SEM (n = 100).

(J) Mitochondria isolated from wild-type, *fcj1*Δ, *mio10*Δ, and *mio27*Δ cells were subjected to hypoosmotic treatment (Swelling) and Proteinase K (Prot. K) digestion where indicated. Samples were analyzed by SDS-PAGE and immunodecoration. See also Figure S4.

proteins analyzed were present in similar amounts in wild-type and *mio10*Δ mitochondria (Figure 4C). No major changes in the steady-state protein levels were observed in *aim5*Δ, *aim13*Δ, *aim37*Δ, and *mio27*Δ mutant mitochondria (Figures S3B–S3D).

We generated yeast strains where Fcj1 was tagged with Protein A and the genes for individual MINOS proteins were deleted (Figures S3E and S3F). Lack of Mio10 led to a nearly complete dissociation of MINOS since the copurification of the other four MINOS components with $Fcj1_{ProtA}$ was strongly decreased (Figure 4D and Figure S3E). Deletion of *AIM5*, *AIM13* and *AIM37* led to a partial dissociation of MINOS with differential effects on the co-isolation of the other MINOS components. Lack of Aim5 considerably destabilized the interaction of MINOS components, whereas loss of Aim13 and Aim37 led to intermediate effects (Figure 4D; Figure S3F). Mio27 was not required for the stable association of other MINOS components with Fcj1 (Figure 4D).

In summary, the analysis of yeast mutants for growth, steady-state protein levels and association of MINOS components suggests that mitofilin/Fcj1 and Mio10 are the core components of MINOS.

Defects of MINOS Alter Inner Membrane Cristae Morphology

We then asked how an impairment of MINOS affects mitochondrial morphology. Examination of the mitochondrial network by fluorescence microscopy revealed a partially altered shape in *aim5*Δ, *aim13*Δ, *aim37*Δ, and *mio10*Δ cells with condensed, fragmented mitochondria that appeared to accumulate in the periphery of the cells (Figure S4A), similar to the mitochondrial morphology observed in *fcj1*Δ cells (Rabl et al., 2009). In *mio27*Δ cells only moderate changes of the mitochondrial network were observed (Figure S4A).

Electron microscopy analysis of wild-type cells showed cristae with tubular or leaf-like shape and connections of cristae with the inner boundary membrane (Figure 5A). In yeast cells lacking Fcj1, mitochondria with an increased inner membrane surface and stacks of lamellar cristae with no apparent connection to the inner boundary membrane were observed as reported (Rabl et al., 2009) (Figure 5B). Morphological analysis of *mio10*Δ cells showed a strikingly similar picture (Figure 5C). Morphological analysis of *aim5*Δ, *aim13*Δ, and *aim37*Δ cells revealed an intermediate phenotype with both mitochondria similar to wild-type and mitochondria with stacked lamellar cristae disconnected from the inner boundary membrane (Figures 5D–5F). No considerable defect of mitochondrial morphology was found in *mio27*Δ cells (Figure 5G). A quantitative analysis revealed that 70%–60% of *fcj1*Δ and *mio10*Δ cell sections showed mitochondria with altered cristae morphology (Figure 5H). Morphologically altered mitochondria were observed in 20%–40% of *aim5*Δ, *aim13*Δ, and *aim37*Δ cell sections. We counted the number of crista junction structures visible per cell section and found an inverse correlation to the number of cell sections with stacked lamellar cristae (Figure 5I). In wild-type cells, ~5 crista junctions

per section were observed, whereas this number was reduced to 1.3–1.6 crista junctions per section in *aim5*Δ, *aim13*Δ, and *aim37*Δ cells. Virtually no crista junctions were observed in *fcj1*Δ (Rabl et al., 2009) and *mio10*Δ cells (Figure 5I). Thus, the extent of inner membrane morphology alteration is most pronounced in cells lacking Fcj1 and Mio10, underlining their central role in MINOS.

We determined the consequences of morphological alterations in *fcj1*Δ and *mio10*Δ mitochondria. In the electron microscopy images, crista junctions were mostly absent. As independent approach, we performed osmotic swelling experiments. In hypoosmotic buffer, the volume of the matrix space of wild-type mitochondria increases strongly by uptake of water and the inner membrane expands by partial unfolding of the cristae tubules, thus rupturing the outer membrane. Soluble proteins of the intermembrane space like Tim13 are released from mitochondria and membrane-anchored proteins facing the intermembrane space like Tim23 become accessible to added protease (Figure 5J, lanes 5 and 7). In both *fcj1*Δ and *mio10*Δ mutant mitochondria, release of intermembrane space proteins and protease accessibility of intermembrane space-exposed proteins were impaired (Figure 5J) (upon lysis of mitochondria with detergent, the proteins were digested by protease; Figure S4B). In contrast, *mio27*Δ mitochondria behaved like wild-type mitochondria upon incubation in hypoosmotic buffer (Figure 5J). We conclude that the inner membrane of *fcj1*Δ and *mio10*Δ mutant mitochondria has a strongly reduced capacity to expand and rupture the outer membrane. As the total inner membrane surface appeared rather increased in *fcj1*Δ and *mio10*Δ compared to wild-type, the most likely explanation for the swelling defect is a disruption of the continuity between cristae membranes and inner boundary membrane.

We induced permeabilization of the outer mitochondrial membrane independently of inner membrane expansion. The pro-apoptotic human protein Bax can permeabilize the outer membrane of wild-type yeast mitochondria, leading to release of soluble intermembrane space proteins (Sanjuán Szklarz et al., 2007), shown here for Tim13 and the intermembrane space form of Mcr1, whereas outer and inner membrane proteins are not released (Figure S4C). In contrast, when *fcj1*Δ and *mio10*Δ mitochondria were incubated with Bax, the major fractions of Tim13 and $Mcr1_{IMS}$ were retained in mitochondria (Figure S4C). Thus, the lack of Fcj1 or Mio10 impairs the release of intermembrane space proteins, indicating a limited diffusion between intracristal space and the intermembrane space part that is located between outer membrane and inner boundary membrane.

Distinct Functions of Mitofilin in Inner Membrane Morphology and Protein Import

The identification of MINOS allowed us to address the question if the morphological alterations in *fcj1*Δ mitochondria were responsible for the observed defects in the MIA pathway. Since *mio10*Δ mitochondria showed similar morphological alterations as *fcj1*Δ mitochondria, we imported the radiolabeled precursor of Tim9 into wild-type and *mio10*Δ mitochondria. In contrast to the import defect in *fcj1*Δ mitochondria (Figure 2), import of Tim9 was not inhibited in *mio10*Δ mitochondria: formation of the Tim9-Mia40 intermediate, analyzed by a nonreducing gel, and transport of Tim9 to a protease-protected location were not diminished in *mio10*Δ mitochondria (Figure 6A). Moreover, the import of Tim9 to a protease-protected location in *aim5*Δ, *aim13*Δ, and *aim37*Δ mitochondria was similar to that into wild-type mitochondria (Figure 6B). Thus, the morphological alterations observed in MINOS-deficient mitochondria do not lead to a defective protein import into the intermembrane space. These findings raised the possibility that mitofilin/Fcj1 plays differential roles in the control of inner membrane morphology and protein import.

On size exclusion chromatography, the TOM complex migrated in the 400–600 kDa range but did not comigrate with MINOS in the MDa range (Figure 3E). Possible explanations are that a putative MINOS-TOM supercomplex is disrupted by the chromatographic separation procedure or that a fraction of Fcj1 can interact with TOM in a MINOS-independent manner. We generated a yeast strain that expressed Aim5 with a Protein A-tag. The MINOS components were efficiently copurified with $Aim5_{ProtA}$. In contrast, Tom40 was only copurified with $Fcj1_{ProtA}$, but not with $Aim5_{ProtA}$ (Figure 6C) (the TOM complex was not altered in the tagged mitochondria; Figure S3G). We thus asked if the entire MINOS was required for the interaction between Fcj1 and the TOM complex. Affinity purifications of $Fcj1_{ProtA}$ from *mio10*Δ mitochondria were analyzed with antibodies against Tom40. Tom40 was recovered in the elution fractions in wild-type and *mio10*Δ mutant (Figure 6D), whereas the co-isolation of MINOS components with $Fcj1_{ProtA}$ was strongly impaired in *mio10*Δ mitochondria (Figure 4D and Figure 6D). Similarly, when Fcj1 was purified from mitochondria lacking Aim5 or Aim13, Tom40 was co-isolated (Figure 6D), whereas the copurification of several MINOS components was impaired (Figure 4D and Figure 6D). Thus, the integrity of MINOS is not required for the Fcj1-TOM interaction.

Mitofilin Interacts with Mia40 and Promotes Protein Import into the Intermembrane Space

We asked if Fcj1 is directly connected to the MIA pathway. The SILAC analysis of Fcj1 affinity purification experiments did not lead to a strong enrichment of Mia40 (Table S1). In case of a transient interaction of Fcj1 and Mia40, the yield of copurification would be considerably lower. We thus examined the $Fcj1_{ProtA}$ affinity purification by western blot analysis for the presence of Mia40 and reproducibly observed small amounts of Mia40 in the eluate, whereas control proteins like $F_1\beta$ and Tim10 were not copurified (Figure 7A). For an independent demonstration, we used a yeast strain where Mia40 was tagged with a histidine-extension (Figure 7B). A fraction of Fcj1 was copurified with tagged Mia40, however, the yield of copurification of Fcj1 was an order of magnitude lower than that of Erv1, the partner protein of Mia40 in the MIA disulfide relay, which was copurified with high efficiency as expected (Stojanovski et al., 2008; Kawano et al., 2009). Control proteins such as porin and Tim23 were not copurified with Mia40 (Figure 7B). These results show that Fcj1 and Mia40 interact with each other, though not in stoichiometric amounts.

Since Fcj1 interacts with the TOM complex, a transient interaction of Fcj1 with Mia40 would help to position Mia40 molecules in vicinity of the TOM complex. Two models could explain how the inner membrane-bound Mia40 contacts incoming precursor

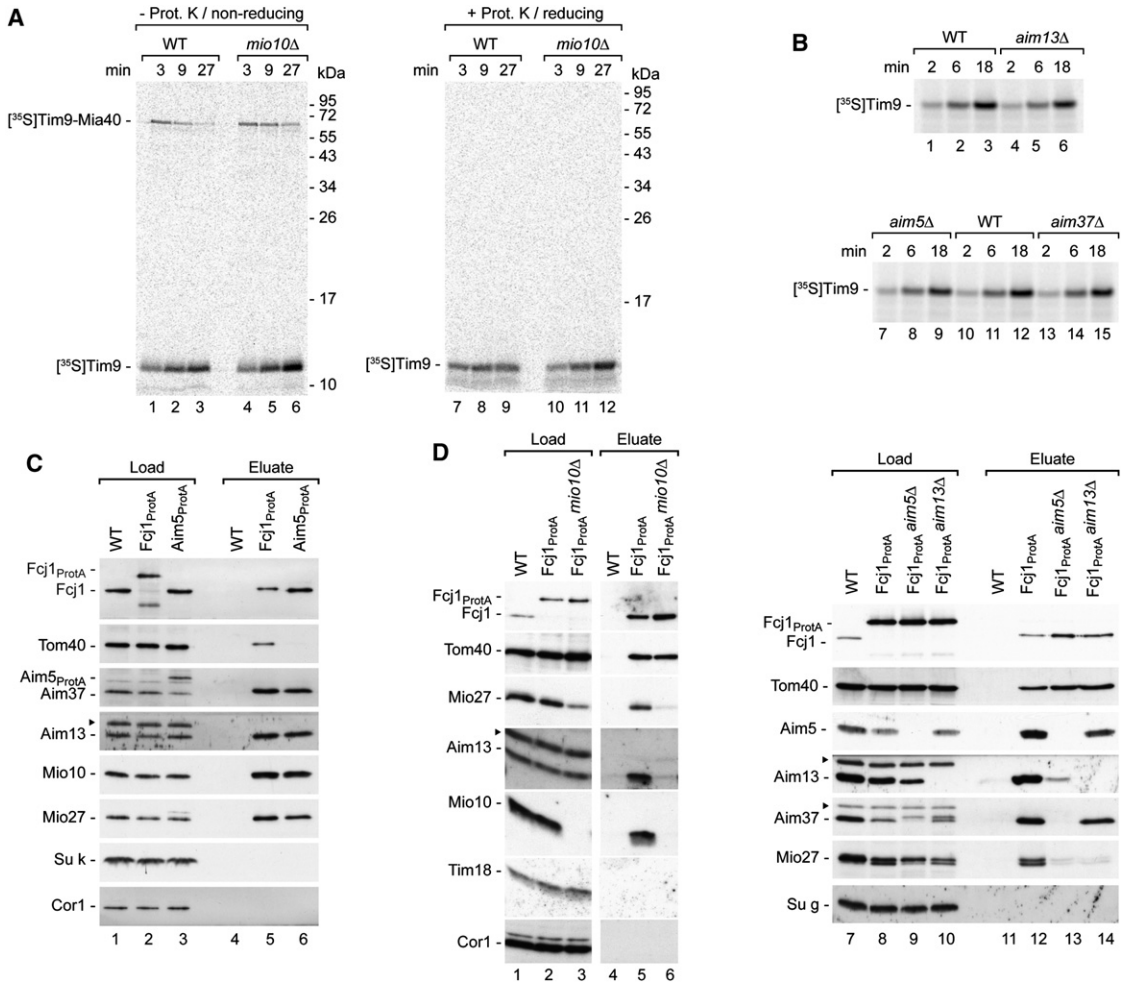

Figure 6. Integrity of MINOS is neither Essential for MIA Pathway nor TOM Interaction

(A) Import of ^{35}S-labeled Tim9 into WT and *mio10Δ* mitochondria, analyzed by reducing or nonreducing SDS-PAGE and autoradiography.

(B) ^{35}S-labeled Tim9 was imported into WT, *aim13Δ*, *aim5Δ*, and *aim37Δ* mitochondria, followed by treatment with proteinase K.

(C) Upon digitonin-solubilization WT, Fcj1$_{ProtA}$ and Aim5$_{ProtA}$ mitochondrial extracts were incubated with IgG-Sepharose beads. Proteins were analyzed by SDS-PAGE and immunodecoration. Arrowhead, unspecific band. Load, 4%; eluate, 100%.

(D) Affinity chromatography using WT, Fcj1$_{ProtA}$, Fcj1$_{ProtA}$ *mio10Δ*, Fcj1$_{ProtA}$ *aim5Δ*, and Fcj1$_{ProtA}$ *aim13Δ* mitochondria performed as in (C).

proteins: (1), MIA substrates may first be fully translocated through the TOM complex into the intermembrane space and then interact with Mia40; or (2), Mia40 is positioned close to the exit site of the TOM channel and binds to precursor proteins during their translocation across the outer membrane. To directly test the second model, we established an assay that dissects the translocation of MIA substrates through the TOM complex. We generated ribosome-nascent chain complexes (RNCs) of Tim9 constructs of various lengths that lacked a stop-codon (Whitley et al., 1996). The constructs were synthesized and radiolabeled in reticulocyte lysates. The ^{35}S-labeled precursor polypeptides were recovered with the ribosomal pellet upon centrifugation through a sucrose cushion and migrated in the 30–40 kDa range on SDS-PAGE (Figure S5A, lane 1). When the Tim9-containing ribosomes were treated with puromycin to release nascent chains, the large Tim9 species disappeared and free Tim9 was generated (Figure S5A, lane 2). The same result was obtained when the ribosomal pellet was treated with RNase A (Figure S5A, lane 4), indicating that the large species represents the ribosome-stalled Tim9-nascent chain bound to a tRNA moiety. When mitochondria were incubated with the ribosome-bound Tim9 constructs, high molecular weight species ranging between ~70–160 kDa were generated (Figure S5B, lane 1). As expected for Mia40 conjugates, these species were sensitive to the reductant DTT (Figure S5B, lane 2). The ~100 kDa species was sensitive to treatment with proteinase K (Figure S5B, lane 4) and RNase A (Figure S5B, lane 8) and was efficiently precipitated with cetyltrimethylammonium bromide (CTAB) (Figure S5B, lane 12), as expected for a tRNA-containing conjugate stalled at the ribosome. In order to demonstrate that the 100 kDa species was bound to Mia40, we used the *mia40-3* allele that generates a C-terminally truncated Mia40. With *mia40-3* mitochondria, the species indeed migrated faster on nonreducing SDS-PAGE (Figure S5C), confirming that it represents the RNC-Mia40

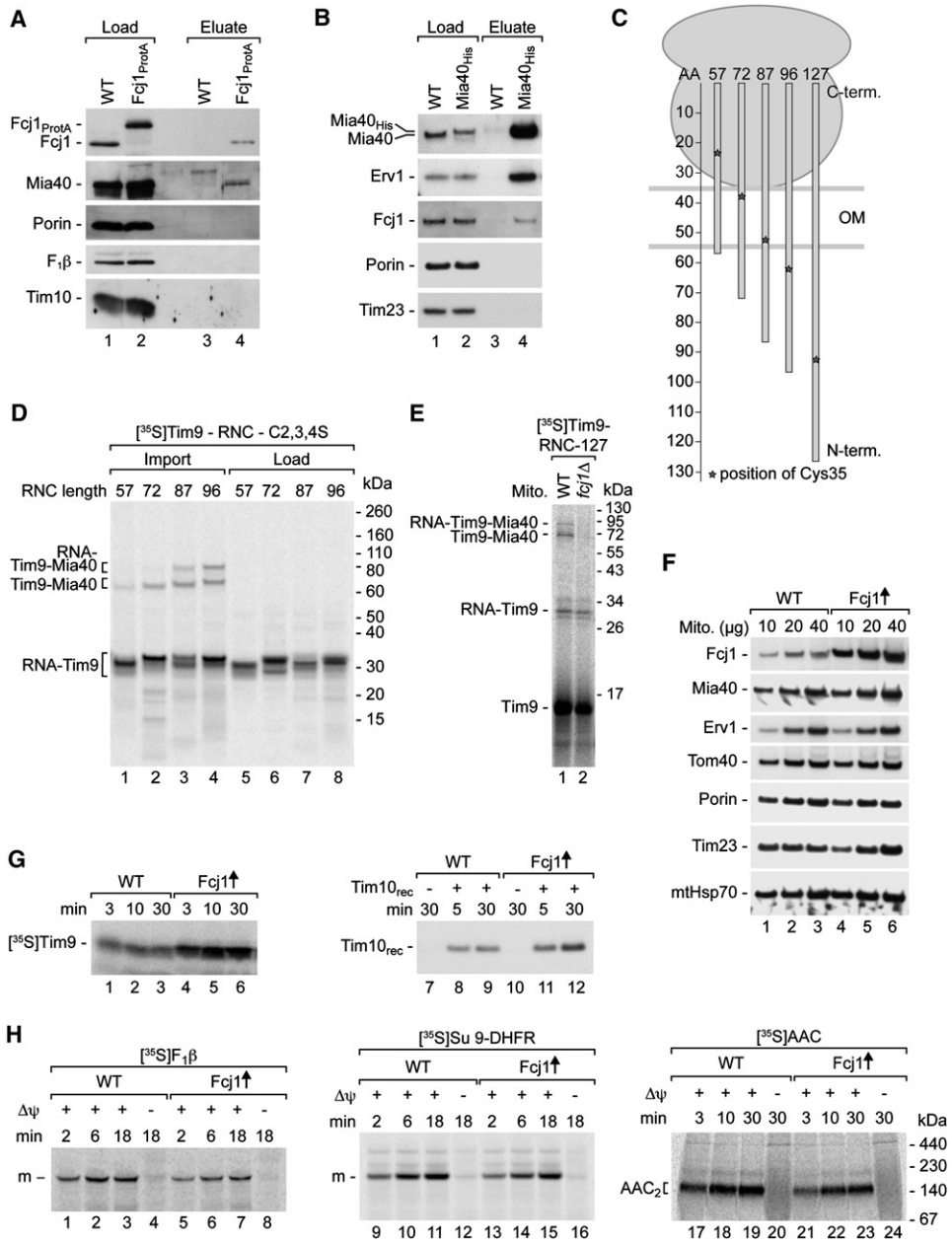

Figure 7. Mitofilin/Fcj1 Recruits Mia40 and Stimulates Protein Import via the MIA Pathway

(A) WT and $Fcj1_{ProtA}$ mitochondria were solubilized in digitonin buffer. Complexes containing Fcj1 were purified by IgG affinity chromatography and analyzed by SDS-PAGE and immunoblotting. Load, 4%; eluate, 100%.

(B) Wild-type and $Mia40_{His}$ mitochondria were lysed with digitonin. Mitochondrial extracts were subjected to Ni^{2+}-NTA affinity chromatography and analyzed by NuPAGE and immunoblotting. Load, 1%; eluate, 100%.

(C) Schematic representation of different lengths of Tim9-RNC constructs stalled at ribosomes.

(D) Tim9-RNCs-C2,3,4S of different lengths were incubated with wild-type mitochondria for 5 min. The samples were analyzed by nonreducing NuPAGE and autoradiography. Load, 10% of RNCs used for the import reactions.

(E) Tim9-RNC-127 was incubated with wild-type and *fcj1Δ* mitochondria for 15 s and analyzed by nonreducing SDS-PAGE.

(F) Steady-state levels of mitochondrial proteins isolated from wild-type and Fcj1 overproducing cells analyzed by NuPAGE and immunoblotting.

(G) Import of ^{35}S-labeled Tim9 and recombinant $Tim10_{His}$ into mitochondria from wild-type and Fcj1 overproducing cells, analyzed by treatment with proteinase K, SDS-PAGE, and autoradiography (lanes 1–6) or immunodecoration (lanes 7–12).

(H) ^{35}S-labeled $F_1\beta$, Su9-DHFR, and AAC were imported into mitochondria. Import reactions were analyzed by treatment with proteinase K and SDS-PAGE (lanes 1–16) or blue native electrophoresis (lanes 17–24). See also Figure S5.

intermediate. Thus, the ribosome-stalled precursor reached through the ribosomal exit tunnel and TOM complex to Mia40 in the intermembrane space.

It has been shown that Mia40 efficiently forms an intermediate with the first cysteine residue of soluble Tim9 (Cys35 of the polypeptide chain) (Milenkovic et al., 2007; Sideris and Tokatlidis, 2007). To examine whether the same is true for Tim9 species stalled at ribosomes, we generated Tim9 constructs where cysteine residues were replaced by serine. Tim9-RNC containing only the first cysteine (cysteines 2, 3, and 4 replaced) formed the Mia40-intermediate like the wild-type precursor (Figure S5D, lanes 6 and 9). We thus used Tim9-C2,3,4S constructs of different length to assess the minimal length of ribosome-stalled precursors required to contact Mia40. The estimated position of the remaining cysteine residue relative to the outer membrane is schematically represented in Figure 7C (Tim9 consists of 87 residues; C-terminal linker residues were added for the longer Tim9 constructs). The assessment is based on a presumed length of the extended nascent precursor of ~35 residues in the ribosomal tunnel and 18–20 residues in the TOM complex (Whitley et al., 1996). Tim9-RNCs were incubated with isolated mitochondria and formation of the Mia40 intermediate was determined by nonreducing SDS-PAGE. Tim9-RNC-57 and Tim9-RNC-72 were not able to form a conjugate with Mia40 (Figure 7D, lanes 1 and 2). However, the Tim9-RNC-87 and Tim9-RNC-96 precursors were capable of engaging with Mia40 (Figure 7D, lanes 3 and 4). With Tim9-RNC-87, the first cysteine residue is just emerging on the intermembrane space side. We conclude that inner membrane-anchored Mia40 is positioned in close vicinity to the TOM channel. Interaction of Mia40 with the precursor in transit across the outer membrane was inhibited in *fcj1*Δ mitochondria (Figure 7E).

Since Fcj1 only recruits a fraction of Mia40, we asked if Fcj1 is rate-limiting, i.e., if overexpression of Fcj1 may exert a stimulatory effect on the MIA pathway. We generated a yeast strain that overexpressed Fcj1. The steady state levels of Mia40, Erv1 and control proteins were not altered (Figure 7F). Import of radiolabeled Tim9 as well as purified Tim10 into mitochondria was considerably increased upon overexpression of Fcj1 (Figure 7G). In contrast, neither protein import via the presequence pathway ($F_1\beta$ and the matrix-targeted model protein Su9-DHFR) nor the carrier pathway (AAC) were enhanced by overexpression of Fcj1 (Figure 7H). We conclude that overexpression of Fcj1 stimulates protein import into the intermembrane space via the MIA pathway.

DISCUSSION

We have identified a large protein complex in the mitochondrial inner membrane that contains mitofilin and five partner proteins. This mitochondrial inner membrane organizing system (MINOS) is crucial for maintenance of cristae morphology. Mitofilin also interacts with the outer membrane and supports protein translocation into the intermembrane space. We conclude that mitofilin is a multifunctional regulator of mitochondrial morphology and protein biogenesis.

The six MINOS proteins are inner membrane proteins exposing parts to the intermembrane space. Mitofilin, Mio10, Aim5, Aim37, and Mio27 are integral membrane proteins, whereas Aim13 behaves as peripheral membrane protein (Figure S1). Mitofilin and Mio10 are the core components of MINOS and have been conserved from yeast to humans. Mio10-deficient cells show growth defects and strong changes of mitochondrial cristae morphology, including formation of cristae stacks and loss of crista junctions, like cells lacking mitofilin (John et al., 2005; Rabl et al., 2009; Mun et al., 2010). Mio10 is crucial for the architecture of MINOS since a lack of Mio10 disrupts the association of mitofilin with all other MINOS components. Aim5, Aim13, and Aim37, which were initially found in a large screen for genes affecting mitochondrial inheritance (Hess et al., 2009), are also involved in maintenance of the MINOS complex and cristae morphology. Yeast mutants lacking any of these Aim proteins show partial defects of MINOS architecture and mitochondrial inner membrane morphology. Mio27 is homologous to Aim37, yet deletion of its gene did not reveal detectable defects.

Previous studies reported different views on potential partner proteins of mitofilin. (1) Two major mitofilin studies concluded that mitofilin forms a large complex via homotypic interactions (John et al., 2005; Rabl et al., 2009). (2) Head et al. (2011) identified three *Caenorhabditis elegans* proteins that affect mitochondrial morphology in an RNA interference screen, mitofilin, MOMA-1 (*m*itochondrial *o*uter *m*embrane *a*bnormal) and CHCH-3 (coiled-coil *h*elix *c*oiled-coil *h*elix domain-containing protein 3), yet did not show a physical interaction between the proteins. *moma-1* mutants show defects in cristae morphology similar to mitofilin mutants and MOMA-1 has been conserved from yeast to humans (Head et al., 2011). The yeast homologs are Aim37 and Mio27 (Figure S1). The bulk of MOMA-1, however, was localized to the mitochondrial outer membrane by tagging and protease protection assays (Head et al., 2011). We performed a detailed localization of authentic/untagged Aim37 and Mio27 and demonstrate that both proteins are integral proteins of the inner membrane. (3) In further studies, various interaction partners of mitofilin have been proposed, though different stringencies were applied to the specificity of the copurification/comigration approaches (Xie et al., 2007; Mun et al., 2010; Darshi et al., 2011). The protein ChChd3/CHCH-3 was found in two different approaches, copurification with mitofilin in humans (Xie et al., 2007; Darshi et al., 2011) and as genetic interactor of mitofilin in *C. elegans* (Head et al., 2011). Aim13 and ChChd3/CHCH-3, which are both peripheral inner membrane proteins, are not homologs but share a related C-terminal motif with conserved cysteines (CHCH motif; Figure S1), supporting the view that ChChd3/CHCH-3 may be part of MINOS in higher eukaryotes.

Our study defines three classes of MINOS proteins. The first class includes the two core components mitofilin and Mio10. Each of these proteins is crucial for cristae morphology. The second class includes Aim5, Aim13/ChChd3/CHCH-3, and Aim37/MOMA-1. These proteins are not strictly essential for maintenance of inner membrane morphology, but mutants of a class II protein lead to partial defects in MINOS and cristae morphology. The third class includes proteins like Mio27 that are associated with MINOS but do not lead to defects upon deletion. Since MINOS forms a large complex in the MDa range, it is evident that multiple copies of MINOS components have to be present and thus homotypic interactions of components, as shown for mitofilin (John et al., 2005; Rabl et al., 2009), likely

contribute to the formation of MINOS. Mitofilin is enriched in crista junctions (Rabl et al., 2009). Since crista junctions are lost or their number is diminished in different MINOS mutants, the available results support the view that the large MINOS complex contributes to the maintenance of crista junction structures and is required for keeping cristae membranes attached to the inner boundary membrane. Different models are discussed for the formation of mitochondrial cristae (summarized in Zick et al., 2009). In the invagination model, incorporation of newly synthesized phospholipids into the inner membrane may represent an early step of cristae biogenesis, leading to expansion and invagination of the membrane (Renken et al., 2002). The invaginations are shaped into tubules by oligomers of ATP synthase, Mgm1/OPA1 and possibly also Mdm33 (Messerschmitt et al., 2003; Arnoult et al., 2005; Frezza et al., 2006; Meeusen et al., 2006; Vogel et al., 2006; Merkwirth et al., 2008; Yamaguchi et al., 2008; Zick et al., 2009). MINOS likely functions late in cristae biogenesis since MINOS mutants can respire, generate ATP, and contain inner membranes with an increased surface area (John et al., 2005; Rabl et al., 2009; this study). MINOS may help to anchor the base of cristae tubules at the inner boundary membrane and prevent the release of cristae membranes.

We found that mitofilin plays a further role in mitochondrial protein biogenesis. Mitofilin-deficient mitochondria show defects in the import of MIA substrates into the intermembrane space. Mia40 exposes its large receptor domain to the intermembrane space (Neupert and Herrmann, 2007; Chacinska et al., 2009; Endo et al., 2011). Since the formation of cristae stacks in mitofilin mutant mitochondria leads to segregation of a major part of the intracristal space (John et al., 2005; Rabl et al., 2009; this study), the most obvious explanation would be that also Mia40 is segregated and thus the efficiency of the MIA pathway would be indirectly inhibited due to the morphological alteration of the inner membrane. In contrast to mitofilin-deficient mitochondria, however, Mio10-deficient mitochondria efficiently import MIA substrates, although mutants of both MINOS class I proteins show comparable defects in cristae morphology, supporting the view that mitofilin may play a role in the MIA system.

The mechanistic explanation is provided by the interaction of mitofilin with the TOM complex. Since mitofilin also transiently interacts with Mia40, mitofilin helps to position Mia40 molecules in close vicinity to the protein translocation channel of the outer membrane (Figure S5E). Mia40 functions as trans receptor on the intermembrane space side and specifically binds the first cysteine residues of incoming substrate precursors (Milenkovic et al., 2007; Sideris and Tokatlidis, 2007; Kawano et al., 2009; Bien et al., 2010). Using ribosome-nascent chain complexes, we show that Mia40 interacts with the precursor protein in transit as soon as the first cysteine residue emerges on the intermembrane space side of the TOM complex. Thus, Mia40 has to be in close proximity to the TOM complex in order to capture the precursor protein immediately upon arrival in the intermembrane space. Such a mechanism ensures that the reduced cysteine residue cannot engage in incorrect disulfide bond formation in the intermembrane space (that is less reducing than the cytosol) and thus Mia40 can protect the precursor from nonproductive interaction.

We conclude that mitofilin is a multifunctional protein. The assembly with inner membrane proteins is critical for formation of MINOS and controlling cristae morphology. Additionally, mitofilin interacts with the outer membrane and helps to position Mia40 in close proximity to the protein import site.

EXPERIMENTAL PROCEDURES

Isolation and Fractionation of Mitochondria

Saccharomyces cerevisiae mitochondria were isolated by differential centrifugation (Stojanovski et al., 2007). For testing submitochondrial localization of proteins, mitochondria were diluted in hypoosmotic buffer to permeabilize the outer membrane and subsequently treated with proteinase K. Membrane integration of proteins was analyzed by incubation of isolated mitochondria in 0.1 M Na_2CO_3 and ultracentrifugation to separate membrane-bound and soluble proteins.

Affinity Purification and Mass Spectrometry

For affinity purification of Protein A-tagged proteins mitochondria were solubilized with digitonin and extracts were incubated with IgG-Sepharose beads. Bound proteins were eluted with TEV protease. When SILAC-labeled mitochondria were used, elution fractions from the $^{12}C/^{14}N$ and $^{13}C/^{15}N$ samples were precipitated with acetone, mixed for digestion with trypsin and subjected to mass spectrometric analysis. Histidine-tagged Mia40 was purified by Ni^{2+}-NTA affinity chromatography. Bound proteins were eluted with buffer containing 400 mM imidazole.

Import of Proteins into Mitochondria

Mitochondrial precursor proteins for in vitro import reactions were either synthesized in reticulocyte lysate in the presence of [^{35}S]methionine or recombinantly expressed in *Escherichia coli* and purified. The precursor proteins were incubated with isolated mitochondria (Stojanovski et al., 2007). The mitochondria were re-isolated and analyzed by SDS-PAGE or blue native electrophoresis.

Native Analysis of Protein Complexes

For blue native electrophoresis mitochondria were solubilized in digitonin-containing buffer (1% [w/v] digitonin, 20 mM Tris-HCl, pH 7.4, 0.1 mM EDTA, 50 mM NaCl, 10% [v/v] glycerol, and 1 mM PMSF). After a clarifying spin, 10× loading dye was added and protein complexes were separated on blue native polyacrylamide gradient gels (Stojanovski et al., 2007). For separation of protein complexes by size exclusion chromatography, isolated mitochondria were solubilized in digitonin buffer and applied on a TSK400W column (Tosoh Biosciences, Tokyo, Japan).

Electron Microscopy

For cryosectioning yeast cells were fixed in 1% formaldehyde and 3% glutaraldehyde on ice. For diaminobenzidine staining, yeast cells fixed in 3% glutaraldehyde were incubated in a mixture containing 2 mg/ml diaminobenzidine and 0.06% hydrogen peroxide. Cells were postfixed with 1.5% $KMnO_4$, poststained with 0.5% uranylacetate and embedded in Epon 812.

Generation of Ribosome-Nascent Chain Complexes

Generation of RNCs was performed essentially as described (Gilmore et al., 1991). The *TIM9* open reading frame was amplified by PCR with a forward primer containing an SP6 promoter and a reverse primer allowing for the deletion of the stop codon. Tim9-RNCs of different length specified by the number of amino acid residues (Tim9-RNC-57, -72, -87, -96, -127) were generated by modifying the reverse primer and using different templates. Tim9-RNC-57, Tim9-RNC-72, Tim9-RNC-87 were obtained by amplification of the *TIM9* coding sequence from yeast genomic DNA. Tim9-RNC-96 was obtained from genomic DNA using a reverse primer that contained the sequence for nine additional lysine residues. Tim9-RNC-127 was obtained by using a plasmid (pGEM4Z) coding for Tim9 fused to dihydrofolate reductase (1769). Tim9-RNCs containing cysteine substitutions were derived from plasmids containing mutagenized *TIM9* alleles described in Milenkovic et al. (2007). The following cysteine residues were changed to serine: Tim9-C1S (1580 or

1760), Tim9-C1,4S (1546), Tim9-C2,3,4 (1587), and Tim9-C1,2,3,4S (1548). The obtained PCR products were used for in vitro transcription using the mMESSAGE mMACHINE kit (Ambion) and translation using the Flexi Rabbit Reticulocyte Lysate System (Promega) in the presence of [^{35}S]methionine. Translation reactions were performed for 10–15 min at 20°C. After a clarifying spin at 20,000 × g and 4°C for 15 min, the lysate was loaded on a sucrose cushion (25% sucrose, 20 mM HEPES-KOH, 2 mM magnesium acetate, 120 mM potassium acetate, 1 mM PMSF, pH 7.4) and centrifuged at 355,000 × g at 4°C for 35 min (TLA 120.2 rotor; Beckman Coulter, Brea, CA). The RNC-containing pellets were resuspended in a buffer composed of 20 mM HEPES-KOH, 2 mM magnesium acetate, 100 mM potassium acetate, 1 mM PMSF, 600 mM sorbitol, pH 7.4, and used for further experiments. RNCs were precipitated using hexadecyltrimethylammonium bromide (CTAB) according to Gilmore et al. (1991). Samples were incubated in digitonin/CTAB buffer (20 mM Tris-HCl, pH 7.4, 250 mM sodium acetate, 0.5 mM EDTA, 10% [v/v] glycerol, 50 mM NaCl, 1% [w/v] digitonin, 1 mM PMSF, 50 mM iodoacetamide, 1% [w/v] CTAB) with yeast tRNA (50 μg in a 200 μl reaction) as carrier for 10 min at 30°C. Precipitated material was recovered by centrifugation at 20,000 × g for 15 min. In order to release nascent chains from ribosomes, 3 mM puromycin was added and samples were incubated for 5 min. For digestion of tRNA, RNase A (1:50 diluted; QIAGEN) was added and samples were incubated for 5 min at 25°C.

SUPPLEMENTAL INFORMATION

Supplemental Information includes five figures and one table and can be found with this article online at doi:10.1016/j.devcel.2011.08.026.

ACKNOWLEDGMENTS

We thank Drs. B. Guiard, R. Ieva, J. Nunnari, O. Schmidt, and N. Wiedemann for discussion, Dr. K. Truscott for plasmids, I. Perschil, B. Knapp, and A. Gornicka for experimental assistance, and A. Kram and R. de Boer for assistance with the EM analysis. This work was supported by the Deutsche Forschungsgemeinschaft, Sonderforschungsbereich 746, Excellence Initiative of the German Federal and State Governments (EXC 294 BIOSS; GSC-4 Spemann Graduate School), Bundesministerium für Bildung und Forschung (Dynamo), Gottfried Wilhelm Leibniz Program, Landesforschungspreis Baden-Württemberg, Foundation for Polish Science-Welcome programme cofinanced by the EU Regional Development Fund, EMBO (A.C.), Boehringer Ingelheim Fonds predoctoral fellowship (M.B.), and was carried out within the research program of the Kluyver Centre for Genomics of Industrial Fermentation, which is part of the Netherlands Genomics Initiative/Netherlands Organization for Scientific Research.

Received: July 3, 2011
Revised: August 25, 2011
Accepted: August 29, 2011
Published online: September 22, 2011

REFERENCES

Arnoult, D., Grodet, A., Lee, Y.J., Estaquier, J., and Blackstone, C. (2005). Release of OPA1 during apoptosis participates in the rapid and complete release of cytochrome *c* and subsequent mitochondrial fragmentation. J. Biol. Chem. *280*, 35742–35750.

Bien, M., Longen, S., Wagener, N., Chwalla, I., Herrmann, J.M., and Riemer, J. (2010). Mitochondrial disulfide bond formation is driven by intersubunit electron transfer in Erv1 and proofread by glutathione. Mol. Cell *37*, 516–528.

Chacinska, A., Lind, M., Frazier, A.E., Dudek, J., Meisinger, C., Geissler, A., Sickmann, A., Meyer, H.E., Truscott, K.N., Guiard, B., et al. (2005). Mitochondrial presequence translocase: switching between TOM tethering and motor recruitment involves Tim21 and Tim17. Cell *120*, 817–829.

Chacinska, A., Koehler, C.M., Milenkovic, D., Lithgow, T., and Pfanner, N. (2009). Importing mitochondrial proteins: machineries and mechanisms. Cell *138*, 628–644.

Darshi, M., Mendiola, V.L., Mackey, M.R., Murphy, A.N., Koller, A., Perkins, G.A., Ellisman, M.H., and Taylor, S.S. (2011). ChChd3, an inner mitochondrial membrane protein, is essential for maintaining crista integrity and mitochondrial function. J. Biol. Chem. *286*, 2918–2932.

Dolezal, P., Likic, V., Tachezy, J., and Lithgow, T. (2006). Evolution of the molecular machines for protein import into mitochondria. Science *313*, 314–318.

Endo, T., Yamano, K., and Kawano, S. (2011). Structural insight into the mitochondrial protein import system. Biochim. Biophys. Acta *1808*, 955–970.

Frezza, C., Cipolat, S., Martins de Brito, O., Micaroni, M., Beznoussenko, G.V., Rudka, T., Bartoli, D., Polishuck, R.S., Danial, N.N., De Strooper, B., and Scorrano, L. (2006). OPA1 controls apoptotic cristae remodeling independently from mitochondrial fusion. Cell *126*, 177–189.

Gilkerson, R.W., Selker, J.M.L., and Capaldi, R.A. (2003). The cristal membrane of mitochondria is the principal site of oxidative phosphorylation. FEBS Lett. *546*, 355–358.

Gilmore, R., Collins, P., Johnson, J., Kellaris, K., and Rapiejko, P. (1991). Transcription of full-length and truncated mRNA transcripts to study protein translocation across the endoplasmic reticulum. Methods Cell Biol. *34*, 223–239.

Head, B.P., Zulaika, M., Ryazantsev, S., and van der Bliek, A.M. (2011). A novel mitochondrial outer membrane protein, MOMA-1, that affects cristae morphology in *Caenorhabditis elegans*. Mol. Biol. Cell *22*, 831–841.

Hess, D.C., Myers, C.L., Huttenhower, C., Hibbs, M.A., Hayes, A.P., Paw, J., Clore, J.J., Mendoza, R.M., Luis, B.S., Nislow, C., et al. (2009). Computationally driven, quantitative experiments discover genes required for mitochondrial biogenesis. PLoS Genet. *5*, e1000407.

John, G.B., Shang, Y., Li, L., Renken, C., Mannella, C.A., Selker, J.M.L., Rangell, L., Bennett, M.J., and Zha, J. (2005). The mitochondrial inner membrane protein mitofilin controls cristae morphology. Mol. Biol. Cell *16*, 1543–1554.

Kawano, S., Yamano, K., Naoé, M., Momose, T., Terao, K., Nishikawa, S., Watanabe, N., and Endo, T. (2009). Structural basis of yeast Tim40/Mia40 as an oxidative translocator in the mitochondrial intermembrane space. Proc. Natl. Acad. Sci. USA *106*, 14403–14407.

Mannella, C.A. (2006). The relevance of mitochondrial membrane topology to mitochondrial function. Biochim. Biophys. Acta *1762*, 140–147.

Meeusen, S., DeVay, R., Block, J., Cassidy-Stone, A., Wayson, S., McCaffery, J.M., and Nunnari, J. (2006). Mitochondrial inner-membrane fusion and crista maintenance requires the dynamin-related GTPase Mgm1. Cell *127*, 383–395.

Merkwirth, C., Dargazanli, S., Tatsuta, T., Geimer, S., Löwer, B., Wunderlich, F.T., von Kleist-Retzow, J.C., Waisman, A., Westermann, B., and Langer, T. (2008). Prohibitins control cell proliferation and apoptosis by regulating OPA1-dependent cristae morphogenesis in mitochondria. Genes Dev. *22*, 476–488.

Messerschmitt, M., Jakobs, S., Vogel, F., Fritz, S., Dimmer, K.S., Neupert, W., and Westermann, B. (2003). The inner membrane protein Mdm33 controls mitochondrial morphology in yeast. J. Cell Biol. *160*, 553–564.

Milenkovic, D., Gabriel, K., Guiard, B., Schulze-Specking, A., Pfanner, N., and Chacinska, A. (2007). Biogenesis of the essential Tim9-Tim10 chaperone complex of mitochondria: site-specific recognition of cysteine residues by the intermembrane space receptor Mia40. J. Biol. Chem. *282*, 22472–22480.

Mokranjac, D., Sichting, M., Popov-Celeketić, D., Mapa, K., Gevorkyan-Airapetov, L., Zohary, K., Hell, K., Azem, A., and Neupert, W. (2009). Role of Tim50 in the transfer of precursor proteins from the outer to the inner membrane of mitochondria. Mol. Biol. Cell *20*, 1400–1407.

Mun, J.Y., Lee, T.H.L., Kim, J.H., Yoo, B.H., Bahk, Y.Y., Koo, H.-S., and Han, S.S. (2010). *Caenorhabditis elegans* mitofilin homologs control the morphology of mitochondrial cristae and influence reproduction and physiology. J. Cell. Physiol. *224*, 748–756.

Neupert, W., and Herrmann, J.M. (2007). Translocation of proteins into mitochondria. Annu. Rev. Biochem. *76*, 723–749.

Ong, S.E., and Mann, M. (2006). A practical recipe for stable isotope labeling by amino acids in cell culture (SILAC). Nat. Protoc. *1*, 2650–2660.

Paumard, P., Vaillier, J., Coulary, B., Schaeffer, J., Soubannier, V., Mueller, D.M., Brèthes, D., di Rago, J.-P., and Velours, J. (2002). The ATP synthase is involved in generating mitochondrial cristae morphology. EMBO J. *21*, 221–230.

Rabl, R., Soubannier, V., Scholz, R., Vogel, F., Mendl, N., Vasiljev-Neumeyer, A., Körner, C., Jagasia, R., Keil, T., Baumeister, W., et al. (2009). Formation of cristae and crista junctions in mitochondria depends on antagonism between Fcj1 and Su *e/g*. J. Cell Biol. *185*, 1047–1063.

Renken, C., Siragusa, G., Perkins, G., Washington, L., Nulton, J., Salamon, P., and Frey, T.G. (2002). A thermodynamic model describing the nature of the crista junction: a structural motif in the mitochondrion. J. Struct. Biol. *138*, 137–144.

Sanjuán Szklarz, L.K., Kozjak-Pavlovic, V., Vögtle, F.-N., Chacinska, A., Milenkovic, D., Vogel, S., Dürr, M., Westermann, B., Guiard, B., Martinou, J.C., et al. (2007). Preprotein transport machineries of yeast mitochondrial outer membrane are not required for Bax-induced release of intermembrane space proteins. J. Mol. Biol. *368*, 44–54.

Sideris, D.P., and Tokatlidis, K. (2007). Oxidative folding of small Tims is mediated by site-specific docking onto Mia40 in the mitochondrial intermembrane space. Mol. Microbiol. *65*, 1360–1373.

Strauss, M., Hofhaus, G., Schröder, R.R., and Kühlbrandt, W. (2008). Dimer ribbons of ATP synthase shape the inner mitochondrial membrane. EMBO J. *27*, 1154–1160.

Stojanovski, D., Pfanner, N., and Wiedemann, N. (2007). Import of proteins into mitochondria. Methods Cell Biol. *80*, 783–806.

Stojanovski, D., Milenkovic, D., Müller, J.M., Gabriel, K., Schulze-Specking, A., Baker, M.J., Ryan, M.T., Guiard, B., Pfanner, N., and Chacinska, A. (2008). Mitochondrial protein import: precursor oxidation in a ternary complex with disulfide carrier and sulfhydryl oxidase. J. Cell Biol. *183*, 195–202.

Tamura, Y., Harada, Y., Shiota, T., Yamano, K., Watanabe, K., Yokota, M., Yamamoto, H., Sesaki, H., and Endo, T. (2009). Tim23-Tim50 pair coordinates functions of translocators and motor proteins in mitochondrial protein import. J. Cell Biol. *184*, 129–141.

Tienson, H.L., Dabir, D.V., Neal, S.E., Loo, R., Hasson, S.A., Boontheung, P., Kim, S.-K., Loo, J.A., and Koehler, C.M. (2009). Reconstitution of the mia40-erv1 oxidative folding pathway for the small tim proteins. Mol. Biol. Cell *20*, 3481–3490.

Vogel, F., Bornhövd, C., Neupert, W., and Reichert, A.S. (2006). Dynamic subcompartmentalization of the mitochondrial inner membrane. J. Cell Biol. *175*, 237–247.

Whitley, P., Nilsson, I.M., and von Heijne, G. (1996). A nascent secretory protein may traverse the ribosome/endoplasmic reticulum translocase complex as an extended chain. J. Biol. Chem. *271*, 6241–6244.

Wurm, C.A., and Jakobs, S. (2006). Differential protein distributions define two sub-compartments of the mitochondrial inner membrane in yeast. FEBS Lett. *580*, 5628–5634.

Xie, J., Marusich, M.F., Souda, P., Whitelegge, J., and Capaldi, R.A. (2007). The mitochondrial inner membrane protein mitofilin exists as a complex with SAM50, metaxins 1 and 2, coiled-coil-helix coiled-coil-helix domain-containing protein 3 and 6 and DnaJC11. FEBS Lett. *581*, 3545–3549.

Yamaguchi, R., Lartigue, L., Perkins, G., Scott, R.T., Dixit, A., Kushnareva, Y., Kuwana, T., Ellisman, M.H., and Newmeyer, D.D. (2008). Opa1-mediated cristae opening is Bax/Bak and BH3 dependent, required for apoptosis, and independent of Bak oligomerization. Mol. Cell *31*, 557–569.

Zick, M., Rabl, R., and Reichert, A.S. (2009). Cristae formation-linking ultrastructure and function of mitochondria. Biochim. Biophys. Acta *1793*, 5–19.